A fumarole in a one-pot: synthesis, crystal structure and properties of Zn- and Mg-analogs of itelmenite and a synthetic analog of glikinite

Diana O Nekrasova, Oleg I Siidra, Anatoly N. Zaitsev, Valery L. Ugolkov, Marie Colmont, Dmitry O. Charkin, Olivier Mentré, Ruiqi Chen, Vadim M. Kovrugin, Artem S. Borisov

Dear Author,

Here are the proofs of your article.

- You can submit your corrections **online**, via **e-mail** or by **fax**.
- For **online** submission please insert your corrections in the online correction form. Always indicate the line number to which the correction refers.
- You can also insert your corrections in the proof PDF and **email** the annotated PDF.
- For fax submission, please ensure that your corrections are clearly legible. Use a fine black pen and write the correction in the margin, not too close to the edge of the page.
- Remember to note the **journal title**, **article number**, and **your name** when sending your response via e-mail or fax.
- **Check** the metadata sheet to make sure that the header information, especially author names and the corresponding affiliations are correctly shown.
- **Check** the questions that may have arisen during copy editing and insert your answers/ corrections.
- **Check** that the text is complete and that all figures, tables and their legends are included. Also check the accuracy of special characters, equations, and electronic supplementary material if applicable. If necessary refer to the *Edited manuscript*.
- The publication of inaccurate data such as dosages and units can have serious consequences. Please take particular care that all such details are correct.
- Please **do not** make changes that involve only matters of style. We have generally introduced forms that follow the journal's style.
  Substantial changes in content, e.g., new results, corrected values, title and authorship are not allowed without the approval of the responsible editor. In such a case, please contact the Editorial Office and return his/her consent together with the proof.
- If we do not receive your corrections **within 48 hours**, we will send you a reminder.
- Your article will be published **Online First** approximately one week after receipt of your corrected proofs. This is the **official first publication** citable with the DOI. **Further changes are, therefore, not possible.**
- The **printed version** will follow in a forthcoming issue.

Please note

After online publication, subscribers (personal/institutional) to this journal will have access to the complete article via the DOI using the URL: http://dx.doi.org/[DOI].
If you would like to know when your article has been published online, take advantage of our free alert service. For registration and further information go to: http://www.link.springer.com.

Due to the electronic nature of the procedure, the manuscript and the original figures will only be returned to you on special request. When you return your corrections, please inform us if you would like to have these documents returned.

Metadata of the article that will be visualized in OnlineFirst

ArticleTitle	A fumarole in a one-pot: synthesis, crystal structure and properties of Zn- and Mg-analogs of itelmenite and a synthetic analog of glikinite	
Article Sub-Title		
Article CopyRight	The Author(s), under exclusive licence to Springer-Verlag GmbH, DE part of Springer Nature (This will be the copyright line in the final PDF)	
Journal Name	Physics and Chemistry of Minerals	
Corresponding Author	Family Name	**Siidra**
	Particle	
	Given Name	**Oleg I.**
	Suffix	
	Division	Department of Crystallography
	Organization	St. Petersburg State University
	Address	University Embankment 7/9, 199034, St. Petersburg, Russia
	Division	Institute of Silicate Chemistry
	Organization	Russian Academy of Sciences
	Address	Makarov Emb. 2, 199034, St. Petersburg, Russia
	Phone	
	Fax	
	Email	o.siidra@spbu.ru
	URL	
	ORCID	http://orcid.org/0000-0003-1908-3152
Author	Family Name	**Nekrasova**
	Particle	
	Given Name	**Diana O.**
	Suffix	
	Division	Department of Crystallography
	Organization	St. Petersburg State University
	Address	University Embankment 7/9, 199034, St. Petersburg, Russia
	Division	
	Organization	Université Lille, CNRS, Centrale Lille, Université Artois, UMR 8181, Unité de Catalyse et Chimie du Solide
	Address	59000, Lille, France
	Phone	
	Fax	
	Email	
	URL	
	ORCID	
Author	Family Name	**Zaitsev**
	Particle	
	Given Name	**Anatoly N.**
	Suffix	

	Division	Department of Mineralogy
	Organization	St. Petersburg State University
	Address	University Embankment 7/9, 199034, St. Petersburg, Russia
	Phone	
	Fax	
	Email	
	URL	
	ORCID	
Author	Family Name	**Ugolkov**
	Particle	
	Given Name	**Valery L.**
	Suffix	
	Division	Institute of Silicate Chemistry
	Organization	Russian Academy of Sciences
	Address	Makarov Emb. 2, 199034, St. Petersburg, Russia
	Phone	
	Fax	
	Email	
	URL	
	ORCID	
Author	Family Name	**Colmont**
	Particle	
	Given Name	**Marie**
	Suffix	
	Division	
	Organization	Université Lille, CNRS, Centrale Lille, Université Artois, UMR 8181, Unité de Catalyse et Chimie du Solide
	Address	59000, Lille, France
	Phone	
	Fax	
	Email	
	URL	
	ORCID	
Author	Family Name	**Charkin**
	Particle	
	Given Name	**Dmitry O.**
	Suffix	
	Division	Department of Chemistry
	Organization	Moscow State University, GSP-1
	Address	Moscow, 119991, Russia
	Phone	
	Fax	
	Email	
	URL	
	ORCID	

Author	Family Name	**Mentré**
	Particle	
	Given Name	**Olivier**
	Suffix	
	Division	
	Organization	Université Lille, CNRS, Centrale Lille, Université Artois, UMR 8181, Unité de Catalyse et Chimie du Solide
	Address	59000, Lille, France
	Phone	
	Fax	
	Email	
	URL	
	ORCID	
Author	Family Name	**Chen**
	Particle	
	Given Name	**Ruiqi**
	Suffix	
	Division	Department of Crystallography
	Organization	St. Petersburg State University
	Address	University Embankment 7/9, 199034, St. Petersburg, Russia
	Phone	
	Fax	
	Email	
	URL	
	ORCID	
Author	Family Name	**Kovrugin**
	Particle	
	Given Name	**Vadim M.**
	Suffix	
	Division	Department of Crystallography
	Organization	St. Petersburg State University
	Address	University Embankment 7/9, 199034, St. Petersburg, Russia
	Phone	
	Fax	
	Email	
	URL	
	ORCID	
Author	Family Name	**Borisov**
	Particle	
	Given Name	**Artem S.**
	Suffix	
	Division	Department of Crystallography
	Organization	St. Petersburg State University
	Address	University Embankment 7/9, 199034, St. Petersburg, Russia
	Phone	

Fax
Email
URL
ORCID

Schedule		
	Received	30 March 2020
	Revised	
	Accepted	11 December 2020

Abstract

Anhydrous sulfate minerals are abundant in the active fumaroles with highly oxidizing conditions on the scoria cones of the Tolbachik volcano. The mineral itelmenite, ideally $Na_2CuMg_2(SO_4)_4$, containing isomorphous admixture of Zn, was described in 2018, whereas glikinite, ideally $Zn_3O(SO_4)_2$, was described in 2020. Synthetic analogs of both minerals were obtained during studies of phase formation in the Na_2SO_4–$CuSO_4$–$MgSO_4$–($ZnSO_4$) systems which lead to essentially different results. Solid-state syntheses resulted in formation of several compounds previously known as minerals only. Both Zn- and Mg-containing analogs of itelmenite were prepared and exhibit slight deviations from the ideal $Na_2CuM_2(SO_4)_4$ stoichiometry. The Mg compound could be prepared single-phase which allowed the study of its thermal expansion and IR spectroscopy. $Na_2CuMg_2(SO_4)_4$ and $Na_2CuZn_2(SO_4)_4$ were evaluated for Na^+-ion diffusion. For the Zn compound, several by-products were observed which are synthetic analogs of puninite $Na_2Cu_3O(SO_4)_2$, as well as hermannjahnite $CuZn(SO_4)_2$ and glikinite-type $(Zn,Cu)_3O(SO_4)_2$. All of them were prepared via solid-state reactions in open systems. The $Na_2CuMg_2(SO_4)_4$, $Na_2CuZn_2(SO_4)_4$ and $(Zn,Cu)_3O(SO_4)_2$ were structurally characterized by the single-crystal XRD. In the Zn-bearing system, the admixture of Cu^{2+} likely controls the formation of itelmenite-type and glikinite-type phases. The results of the experiments allowed to deduce possible scenarios of the formation processes of itelmenite and some other endemic fumarolic minerals. Our study shows that outstanding mineralogical diversity observed in the fumaroles of the Tolbachik scoria cones is not only due to the formation from the gas enriched by transition metals and involves also intensive exchange with the host basaltic scoria. The similar processes seem also to be responsible for the recrystallization of many other mineral species observed in high-temperature fumaroles resulted from the recent eruptions.

Keywords (separated by '-')

Anhydrous sulfates - Fumarolic mineral assemblages - $MgSO_4$ - $ZnSO_4$ - Solid-state reactions - Itelmenite - Glikinite - Hermannjahnite - Puninite - Framework structures - X-ray diffraction

Footnote Information

Supplementary Information The online version contains supplementary material available at https://doi.org/10.1007/s00269-020-01132-4.

Physics and Chemistry of Minerals _####################_
https://doi.org/10.1007/s00269-020-01132-4

ORIGINAL PAPER

A fumarole in a one-pot: synthesis, crystal structure and properties of Zn- and Mg-analogs of itelmenite and a synthetic analog of glikinite

Diana O. Nekrasova[1,2] · Oleg I. Siidra[1,3] · Anatoly N. Zaitsev[4] · Valery L. Ugolkov[3] · Marie Colmont[2] · Dmitry O. Charkin[5] · Olivier Mentré[2] · Ruiqi Chen[1] · Vadim M. Kovrugin[1] · Artem S. Borisov[1]

Received: 30 March 2020 / Accepted: 11 December 2020

Abstract

Anhydrous sulfate minerals are abundant in the active fumaroles with highly oxidizing conditions on the scoria cones of the Tolbachik volcano. The mineral itelmenite, ideally $Na_2CuMg_2(SO_4)_4$, containing isomorphous admixture of Zn, was described in 2018, whereas glikinite, ideally $Zn_3O(SO_4)_2$, was described in 2020. Synthetic analogs of both minerals were obtained during studies of phase formation in the Na_2SO_4–$CuSO_4$–$MgSO_4$–($ZnSO_4$) systems which lead to essentially different results. Solid-state syntheses resulted in formation of several compounds previously known as minerals only. Both Zn- and Mg-containing analogs of itelmenite were prepared and exhibit slight deviations from the ideal $Na_2CuM_2(SO_4)_4$ stoichiometry. The Mg compound could be prepared single-phase which allowed the study of its thermal expansion and IR spectroscopy. $Na_2CuMg_2(SO_4)_4$ and $Na_2CuZn_2(SO_4)_4$ were evaluated for Na^+-ion diffusion. For the Zn compound, several by-products were observed which are synthetic analogs of puninite $Na_2Cu_3O(SO_4)_2$, as well as hermannjahnite $CuZn(SO_4)_2$ and glikinite-type $(Zn,Cu)_3O(SO_4)_2$. All of them were prepared via solid-state reactions in open systems. The $Na_2CuMg_2(SO_4)_4$, $Na_2CuZn_2(SO_4)_4$ and $(Zn,Cu)_3O(SO_4)_2$ were structurally characterized by the single-crystal XRD. In the Zn-bearing system, the admixture of Cu^{2+} likely controls the formation of itelmenite-type and glikinite-type phases. The results of the experiments allowed to deduce possible scenarios of the formation processes of itelmenite and some other endemic fumarolic minerals. Our study shows that outstanding mineralogical diversity observed in the fumaroles of the Tolbachik scoria cones is not only due to the formation from the gas enriched by transition metals and involves also intensive exchange with the host basaltic scoria. The similar processes seem also to be responsible for the recrystallization of many other mineral species observed in high-temperature fumaroles resulted from the recent eruptions.

Keywords Anhydrous sulfates · Fumarolic mineral assemblages · $MgSO_4$ · $ZnSO_4$ · Solid-state reactions · Itelmenite · Glikinite · Hermannjahnite · Puninite · Framework structures · X-ray diffraction

Introduction

Minerals containing sulfate anions constitute one of the most diverse groups in terrestrial environments (Alpers et al. 2000). About 400 species bearing SO_4^{2-} group are known to date. Most of the known sulfates are hydrates. A typical

Supplementary Information The online version contains supplementary material available at https://doi.org/10.1007/s00269-020-01132-4.

✉ Oleg I. Siidra
o.siidra@spbu.ru

[1] Department of Crystallography, St. Petersburg State University, University Embankment 7/9, 199034 St. Petersburg, Russia

[2] Université Lille, CNRS, Centrale Lille, Université Artois, UMR 8181, Unité de Catalyse et Chimie du Solide, 59000 Lille, France

[3] Institute of Silicate Chemistry, Russian Academy of Sciences, Makarov Emb. 2, 199034 St. Petersburg, Russia

[4] Department of Mineralogy, St. Petersburg State University, University Embankment 7/9, 199034 St. Petersburg, Russia

[5] Department of Chemistry, Moscow State University, GSP-1, Moscow 119991, Russia

characteristic of anhydrous sulfates with alkali (and transition) metals is their high solubility.

Due to the fast-growing demands in new materials for various energy storage applications, various sulfate compounds have also been studied as promising electrode materials exhibiting relatively stable frameworks (their easy hydration remains a tremendous problem) and higher operating voltages (Barpanda 2015; Lander et al. 2018). Sulfates of sodium and some 3*d*-transition metals are extensively studied as promising materials for efficient Na-ion batteries. From structural viewpoint, the majority of these are synthetic analogs of known minerals. For example, sulfate of sodium and ferric iron, $NaFe(SO_4)_2$, was first discovered as a mineral eldfellite in 2009 (Balić Žunić et al. 2009) in a fumarole of Eldfell volcano, Iceland. Later (Singh et al. 2015), electrochemical properties were investigated on a full synthetic analog. A chemically related alluaudite-type sulfate of sodium and ferrous iron, $Na_2Fe_2(SO_4)_3$ (Barpanda et al. 2014) demonstrates outstanding electrochemical properties (3.8 V vs. Na^+/Na). A known disadvantage of minerals is the presence of impurities (due to both isomorphous substitution and by-phases), which does not allow detailed (and reproducible) studies of their physical properties.

There are but few geological environments on Earth where anhydrous alkali–transition metal sulfates can be found as mineral species: natural coal fires (e.g., Ravat, Tajikistan (Sharygin et al. 2009; Pautov et al. 2020)) and high-temperature volcanic fumaroles (Vergasova and Filatov 2012; Siidra et al. 2017). One of the largest numbers of active volcanoes is located at the Kamchatka Peninsula, Russia. The most interesting from a mineralogical point of view and relatively well studied are the fumaroles with highly oxidizing conditions on the scoria cones of the Tolbachik volcano (Pekov et al. 2018a). In the last century, eruptions on Tolbachik occurred in 1975–1976 (Fedotov and Markhinin, 1983); the most recently in 2012–2013 (Belousov et al. 2015). Of many new mineral species discovered in the past 30 years, the majority has no chemical and structural analogs reported among synthetic materials (Pekov et al. 2018b). The mineral itelmenite, ideally $Na_2CuMg_2(SO_4)_4$, containing isomorphous admixture of Zn, was described in 2018 (Nazarchuk et al. 2018); it was found in the fumarole on the Naboko scoria cone formed during the recent 2012–2013 eruption. Glikinite, ideally $Zn_3O(SO_4)_2$ (Nazarchuk et al. 2020), was collected from the sulfate zone of the arsenic-rich (or As-containing) Arsenatnaya fumarole on the Second scoria cone of the 1975–1976 eruption. Itelmenite exhibits not only a new structure type, but also a new stoichiometry for anhydrous sulfates with alkali and transition metals: $A^+_2M^{2+}_3(SO_4)_4$. Glikinite has a synthetic structural analog (Bald and Grühn 1981); however, the mineral (Nazarchuk et al. 2020) contains essential amount of copper impurity. Synthetic analogs of both these mineral species were obtained in our studies of the Na_2SO_4–$CuSO_4$–MSO_4 (M = Mg, Zn) systems aimed at new possible materials for Na^+-based batteries.

Despite the low conductive ability of the itelmenite-type $Na_2CuM_2(SO_4)_4$ framework, the results on phase formation in the Na_2SO_4–$CuSO_4$–$MgSO_4$–($ZnSO_4$) system appeared interesting with implications to mineralogy and geochemistry. Identified phases mimic fumarolic minerals assemblages, which allowed to deduce some of the secrets of the mineral formation in active fumaroles in scoria cones of Tolbachik volcano.

Synthesis

$Na_2CuMg_2(SO_4)_4$

Initially. a mixture of Na_2SO_4 (Alfa Aesar, 99%), $CuSO_4$ (Prolabo, 98%) and $MgSO_4$ (Alfa Aesar, 99%) reagents were taken in 1:1:2 ratio and were loaded into a platinum crucible and kept at 600 °C for 3 h in air and subsequently cooled for 9 h to room temperature. The product consisted of light-gray crystals and gray powder. Powder XRD analysis revealed the desired $Na_2CuMg_2(SO_4)_4$ and unreacted $MgSO_4$. According to the starting stoichiometry, other (probably poorly crystallized) Na-containing products should also coexist. A single-phase specimen, ideally $Na_2CuMg_2(SO_4)_4$, was successfully synthesized only after the single-crystal XRD and the refinement of the crystal structure reported in detail below. Taking into account the refined occupancies of each site, we were able to prepare the pure product starting from Na_2SO_4, $CuSO_4$ and $MgSO_4$ in 1:1.09:1.91 ratio. Taking in account the mixed occupancies of all *M* sites, one can expect a certain homogeneity range which was not investigated.

Thermal analysis (STA 429 CD NETZSCH) was performed to determine the crystallization temperatures of the Mg and Zn compounds. The powders (ca. 23 mg) were pressed into pellets (5.05 mm diameter and 0.7–0.8 mm height) using a steel die (pressure 1 kg/mm^2). This technique, in comparison to using powdered samples, provides better reproducibility and precision of results. After weighing with precision of ± 10 μg, each pellet was loaded into a Pt–Rh crucible and mounted on a holder, after which TGA study was run at the heating rate of 20 °C /min in a dynamic atmosphere (air flow at 50 cm^3/min) from 40 to 800–900 °C; cooling was performed down to 200 °C at the same rate. The gaseous decomposition products were analyzed on a QMS 403 C NETZSCH quadrupole mass spectrometer operating in a 1–121 m/*z* range.

Figure 1a represents TG, DSC, and IC (ionic currents at $m/z = 18$ and 48, which correspond to H_2O^+ and SO^+)

Journal : Large 269 | Article No : 1132 | Pages : 14 | MS Code : 1132 | Dispatch : 28-12-2020

registered for a pelletized mixture of Na_2SO_4, $CuSO_4$, and $MgSO_4$ taken with the ratio described above upon heating from 40 to 850 °C and cooling to 720 °C.

The low-temperature part of TG curve exhibits two kinks due to mass loss: 1.33% at 56–95 °C, and 1.70% at 172–276 °C which are reflected as endothermic effects on the DSC curve with one maximum at 75 °C for the first one and two maxima at 214 and 241 °C for the second one, respectively. These are accompanied by the maxima for the $m/z = 18$ IC curve. Between the kinks, a monotonous mass loss of 1.04% is observed. The event at 214 °C may be related to partial melting of the sample.

These low-temperature effects clearly occur due to the dehydration processes. We note that the starting material rapidly absorbs water from humid air, most likely with formation of crystalline hydrates (Siidra et al. 2019), even when shortly exposed during opening the container and mounting onto the holder to the TGA apparatus. Note that water is an essential constituent of fumarolic gases (Chaplygin et al. 2016) therefore the experimental conditions still mimic the natural ones.

Further heating the sample proceeds eventlessly from 276 to 560 °C, after which a weak exothermic effect is observed with a maximum at 604 °C. At 617–653 °C, two endothermic effects are observed with maxima at 628 and 648 °C, which are accompanied by weight losses of 0.22%. We attribute a complicated series of effects to crystallization of $Na_2CuMg_2(SO_4)_4$. HT X-ray diffraction study of the reagent mixture (not represented herein) also confirms the appearance of itelmenite in this temperature range. Thus, the crystallization temperature of this compound is in a good agreement with the temperature of gases (600–620 °C) in Saranchinaitovaya fumarole where itelmenite was discovered in 2014 (Nazarchuk et al. 2018) yielding a good emulation of natural fumarolic processes.

The rate of mass loss increases essentially above 653 °C; further heating to 850 °C results in loss of 7.26% accompanied by a strong endothermic effect on the DSC curve (with a maximum at 767 °C and completion at 799 °C. The IC for $m/z = 48$ is observed only above 767 °C when the sample is almost completely melted. After that, the content of sulfur oxides in the decomposition products increases; this indicates that decomposition of sulfates occurs only after complete melting of the sample. It is reasonable to assume that the endothermal effect is due to the sample melting accompanied by the partial decomposition and evolution of sulfur oxides.

Cooling from 850 to 690 °C results in additional mass loss of 1.94%; the DSC curve shows a strong peak at 765 °C due to crystallization, after which evolution of sulfur oxides had stopped. It is possible that some decomposition products (e.g., polysulfuric acids) condense below 195 °C and do not enter the analyzing chamber of the mass spectrometer.

$Na_2CuZn_2(SO_4)_4$

We used the similar synthetic approach as described above for the Mg end-member compound: Na_2SO_4 (Alfa Aesar, 99%), $CuSO_4$ (Prolabo, 98%) and $ZnSO_4$ (Sigma-Aldrich, 99%) reagents were mixed in the "corrected" 1:1.09:1.91 ratio, as explained above. The mixture was loaded into a platinum crucible and kept at 500 °C (in accordance with thermal analysis data described below) for 1 h in air, followed by cooling for 9 h to room temperature. Visual inspection under an optical microscope revealed four crystalline phases different in color and morphology (Fig. 1c). Each of them was identified by the means of the single-crystal X-ray diffraction and SEM–EDX. Light-green crystalline matrix consisting of the irregularly shaped crystals (Fig. 1c) and formed on the bottom of the crucible was determined as the target $Na_2CuZn_2(SO_4)_4$. Unit-cell parameters of the grass-green prismatic crystals corresponded to the mineral puninite, $Na_2Cu_3O(SO_4)_3$ (Siidra et al. 2017). Closer to the crucible walls and upward, a well-crystallized zone of an orange-brown color (Fig. 1c) is observed. Unit-cell parameters of the two types of crystals in this zone correspond to recently discovered glikinite and synthetic $Zn_3O(SO_4)_2$ (Nazarchuk et al. 2020; Bald and Grühn 1981) and previously known synthetic $Na_2Zn(SO_4)_2$ (Berg and Thorup 2005). Different heating regimes were tried and none of them resulted in the single-phase sample of the $Na_2CuZn_2(SO_4)_4$. Crystal structure description and chemical compositions are reported below only for $Na_2CuZn_2(SO_4)_4$ and $(Zn,Cu)_3O(SO_4)_2$.

Figure 1b shows the thermal analysis results for the pelletized mixture of Na_2SO_4, $CuSO_4$, and $ZnSO_4$ taken in the ratio listed above. The sample was heated from 40 to 800 °C and cooled to 150 °C at the same conditions as the previous one.

The initial heating stage is also accompanied by several essential thermal effects which are accompanied by maxima of the $m/z = 18$ ionic current, *i.e.*, they also correspond to release of absorbed water. Next essential endothermal effects are observed in the 477–526 °C range (corresponding maxima at 485 and 505 °C) accompanied by the mass loss of 0.05%. Crystallization of a multiphase sample (Fig. 1c), containing the desired $Na_2CuZn_2(SO_4)_4$, proceeds at essentially lower temperatures compared to its magnesium-based analog. This process is reflected by two very strong thermal effects. The 526–570 °C range is featureless, and monotonous mass loss is as low as 0.05%. No IC at $m/z = 48$ was observed.

An endothermal event starts at 583 °C, reaching its maximum at 678 °C and completing at 691 °C; the mass loss is 1.40%. This is rather common for decomposition processes, yet no peaks were observed on the IC curves. Most likely, the decomposition products had condensed before the analyzing chamber. Another endothermal process commences between

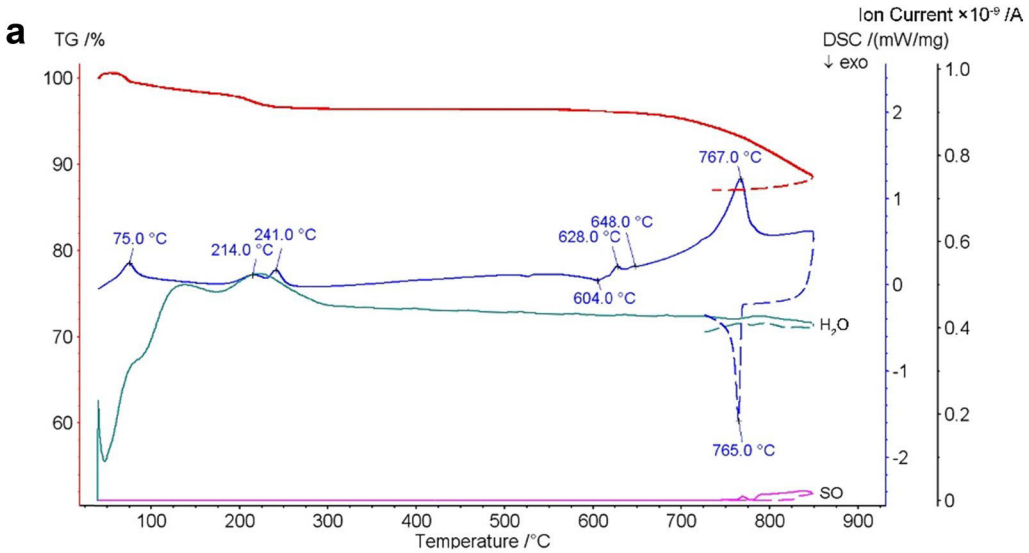

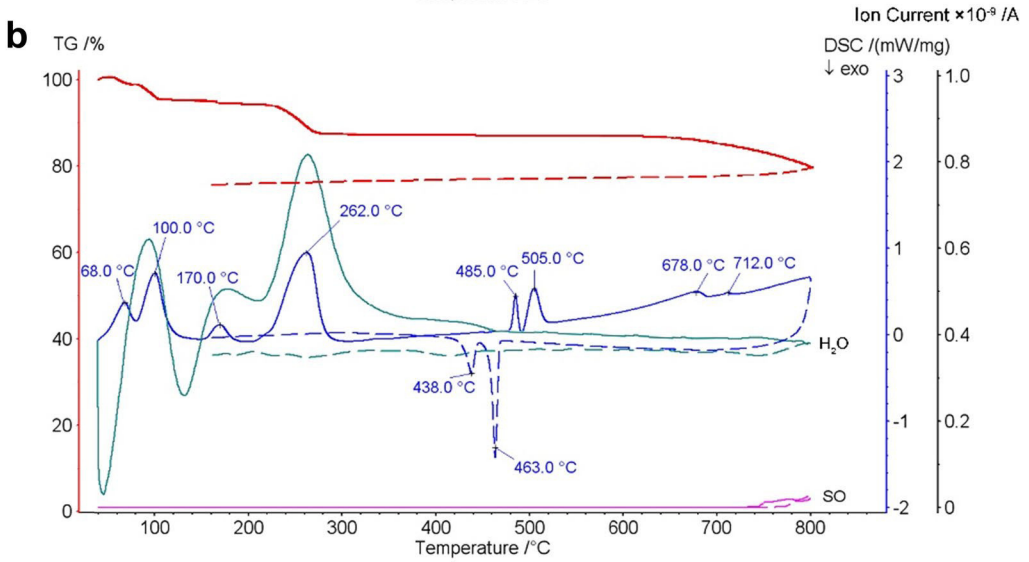

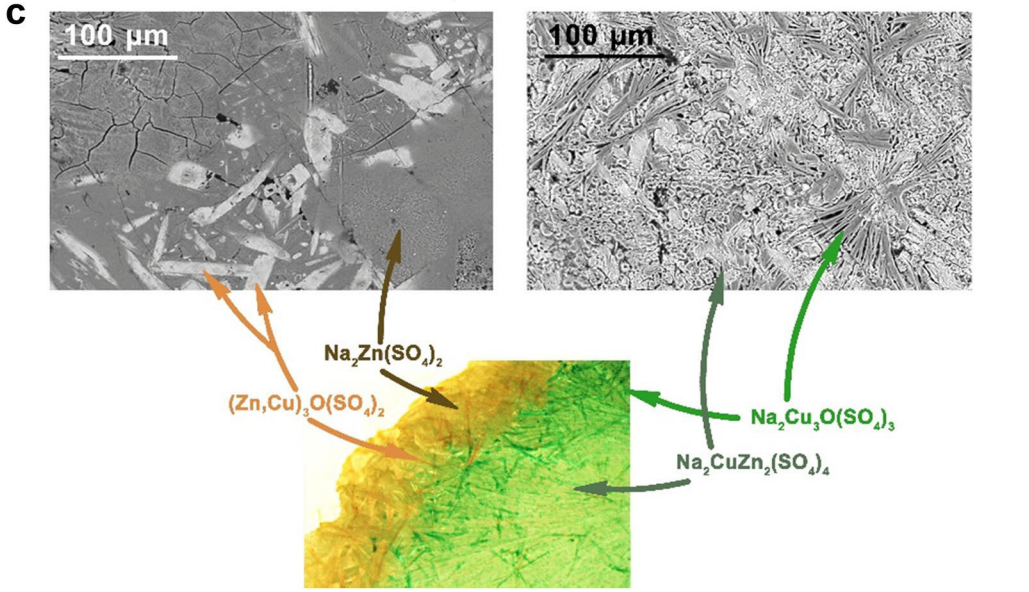

Journal : Large 269 | Article No : 1132 | Pages : 14 | MS Code : 1132 | Dispatch : 28-12-2020

◂**Fig. 1** TG-DSC-IC curves for the mixture of Na_2SO_4, $CuSO_4$ and $MgSO_4$ in 1:1.09:1.91 ratio (**a**). TG-DSC-IC curves for the mixture of Na_2SO_4, $CuSO_4$ and $ZnSO_4$ in 1:1.09:1.91 ratio (**b**). An image of the crucible bottom and wall covered by the various anhydrous sulfates obtained in Na_2SO_4-$CuSO_4$-$ZnSO_4$ system: grass-green needles of $Na_2Cu_3O(SO_4)_3$ (analog of puninite), light-orange needles of $(Zn,Cu)_3O(SO_4)_2$ (analog of glikinite), light-green polycrystalline matrix of $Na_2CuZn_2(SO_4)_4$ (Zn-analog of itelmenite) and light-brown matrix of $Na_2Zn(SO_4)_2$. Two back-scattered electron microscope images of different colored zones are shown above: an orange-colored zone (orange arrows point on light prismatic and isometric crystals of $(Zn,Cu)_3O(SO_4)_2$; a dark-gray matrix consists of $Na_2Zn(SO_4)_2$ and marked by brown arrows) and green zone (sheaf-like dark-gray aggregates of $Na_2Cu_3O(SO_4)_3$ are marked by light-green arrows and dark-green arrows point on multiple irregularly shaped crystals of $Na_2CuZn_2(SO_4)_4$). Ideal formulas are given

691 and 718 °C with a maximum of 712 °C and mass loss of 0.98%. Further heating from 718 to 800 °C resulted in weight loss of 4.63%. No essential effects are observed on the DSC curve, while an ionic current at $m/z = 48$ was registered indicating release of sulfur oxides. It is possible that the decomposition mostly proceeded on the bottom of the Pt crucible.

Upon cooling, the DSC curve features two strong exothermal effects in the 471–417 °C (the corresponding maxima at 463 and 438 °C). These effects may indicate first-order transitions (most likely crystallization of several compounds formed upon heating). As in the previous case, weight loss continued upon cooling from 800 to 700 °C (2.23%).

Chemical composition

Two samples containing ideally $Na_2CuZn_2(SO_4)_4$ and $(Zn,Cu)_3O(SO_4)_2$ were mounted in epoxy resin and polished, to avoid degradation due to atmospheric moisture, without water and oil using a BUELHER CarbiMet P1000, MicroCut P2500 and ChemoMet I. The samples have been studied using a Hitachi S-3400 N scanning electron microscope equipped with an Oxford Instruments X-Max 20 Energy-Dispersive Spectrometer and INCA Wave 500 wavelength dispersive spectrometer. The conditions for energy-dispersive analysis were: accelerating voltage 20 kV, electron beam current 1.0 nA and defocused electron beam (up to 20 μm). The current was measured using a Faraday cup. X-ray acquisition time was 30 s and X-ray processing time '5′ for analysis. System calibration was performed on Co*K*α-*K*β. X-ray matrix correction was carried-out automatically by the Oxford Instruments AZtecTru-Q including an exponential and pile-up correction routine.

The $Na_2(Cu,Zn)_3(SO_4)_4$ compound contains 9.4–10.5 wt.% Na_2O, 25.7–29. wt.% ZnO, 9.2–12.8 wt.% CuO and 50.3–51.8 wt.% SO_3. Hence, the average composition of the phase (13 spot analyses, Table 1), calculated for S = 4, corresponds to $Na_{2.03}Cu_{0.89}Zn_{2.10}(SO_4)_4$ with variation of Zn between 2.00 and 2.24 atoms per formula unit (apfu) and Cu between 0.72 and 1.00 apfu. The general formula can be written as $Na_2(Cu_{1-x}Zn_x)Zn_2(SO_4)_4$ with $x = 0$–0.24.

The $(Zn,Cu)_3O(SO_4)_2$ phase, which occurs along with $Na_2CuZn_2(SO_4)_4$, is Na-free and contains 30.3–36.2 wt.% ZnO, 23.6–28.3 wt.% CuO and 39.4–41.4 wt.% SO_3. Its average composition (11 spot analyses, Table 1), calculated for $S = 2$, is $(Zn_{1.68}Cu_{1.31})O(SO_4)_2$ and general phase formula can be written as $(Zn_{3-x}Cu_x)O(SO_4)_2$, with $x = 1.20$–1.45.

In addition, the studied samples contain another Zn-Cu–S phase (ZnO = 26.3–27.6 wt.%, CuO = 21.3–22.6 wt.% and SO_3 = 49.1–49.7 wt.%, 5 spot analyses (Table 1) with average formula of $Zn_{1.08}Cu_{0.90}(SO_4)_2$ and a Na-Zn-Cu sulfate (Na_2O = 18.5–20.0 wt.%, ZnO = 21.0–24.0 wt.%, CuO = 3.2–5.7 wt.% and SO_3 = 52.4–53.0 wt.%, 6 spot analyses, Table 1) with average formula of $Na_{1.95}(Zn_{0.85}Cu_{0.20})(SO_4)_2$. Both phases were not studied using XRD or single-crystal analysis; the former probably corresponds to mineral hermannjahnite $CuZn(SO_4)_2$ (Siidra et al. 2018) and the latter has no analog among known minerals. $Na_2Zn(SO_4)_2$ (Berg and Thorup 2005) is known for synthetic compounds only.

Powder X-ray diffraction of $Na_2CuMg_2(SO_4)_4$

The X-ray powder diffraction pattern of $Na_2CuMg_2(SO_4)_4$ polycrystalline sample, obtained from Na_2SO_4, $CuSO_4$ and $MgSO_4$ in 1:1.09:1.91 ratio, was collected at room temperature on a laboratory powder diffractometer (Rigaku Ultima IV, CuKα radiation). Data were collected with a step of 0.02° 2Θ using a scanning speed of 3 s per step from 7° to 130°

Table 1 Average compositions (wt. %) of $Na_2CuZn_2(SO_4)_4$, $(Zn,Cu)_3O(SO_4)_2$, $CuZn(SO_4)_2$ and $Na_2Zn(SO_4)_2$

Component	$Na_2CuZn_2(SO_4)_4$	$(Zn,Cu)_3O(SO_4)_2$	$CuZn(SO_4)_2$	$Na_2Zn(SO_4)_2$
Na_2O	10.01	Bld	bld	19.07
ZnO	27.20	34.20	27.11	21.83
CuO	11.21	26.11	21.92	5.16
SO_3	50.90	40.12	49.37	52.66
Total	99.32	100.43	98.40	98.72

Bld below detection limit

2Θ. The program JANA2006 (Petříček et al. 2014) was used to refine the crystal structure. The background was fitted using Chebyshev polynomial function, and the peak shapes were described by a Pseudo-Voigt function. The refined unit-cell parameters of $Na_2CuMg_2(SO_4)_4$ in *Pbca* space group are: $a = 9.5506(1)$ Å, $b = 8.7643(1)$ Å, $c = 28.7100(1)$ Å and $V = 2403.2(1)$ Å^3, $R_P = 2.84\%$. The final observed, calculated, and difference powder XRD pattern resulting from the profile-matching procedure is plotted in Figure S1 which validates a single-phase sample.

Infrared spectroscopy of $Na_2CuMg_2(SO_4)_4$

In order to obtain infrared (IR) absorption spectra for the present study, powdered sample of $Na_2CuMg_2(SO_4)_4$, obtained from Na_2SO_4, $CuSO_4$ and $MgSO_4$ in 1:1.09:1.91 ratio, was mixed with dried KBr, pelletized and analyzed from 4000 to 400 cm^{-1} using a Bruker Vertex 70 spectrometer (Bruker Optics) with a resolution of 4 cm^{-1} and 64 scans. The IR spectrum of an analogous pellet of pure KBr was used as a reference.

The IR spectrum of preliminary heat treated (to avoid hydration) $Na_2CuMg_2(SO_4)_4$ contains three groups of strong bands (in the ranges 464–496, 605–674 and 993–1277 cm^{-1}) (Figure S2). Most of the observed peaks correspond to optically active modes of the three symmetrically independent SO_4 tetrahedra (Smith and Seshadri 1999). The peaks from 464 to 496 cm^{-1} can be tentatively assigned to Mg-O vibrations. The frequencies of the Cu–O stretching and O–Cu–O bending modes are out of the investigated region, i.e., 150–350 cm^{-1} (Secco 1988).

Thermal analysis of $Na_2CuMg_2(SO_4)_4$

Thermal analysis of $Na_2CuMg_2(SO_4)_4$ was performed using a TGA 92–1600 SETARAM analyzer from room temperature to 650 °C (Figure S3). TGA curve demonstrates the stability up to 650 °C. However, one should note at ~ 50 °C a 7–8 weight % loss, assigned to adsorbed H_2O, a systematic drawback dealing with sulfates (Fig. 2).

High-temperature X-ray diffraction of $Na_2CuMg_2(SO_4)_4$

Thermal expansion of $Na_2CuMg_2(SO_4)_4$ was studied in air by means of a Rigaku Ultima X-ray diffractometer (Co*K*α radiation) with a high-temperature camera Rigaku HTA 1600. The sample was prepared from heptane's suspension on a Pt–Rh plate. The temperature step was 50 °C in the range 50–400 °C and 20 °C in the range of 400–680 °C. Unit-cell parameters at different temperatures were refined by least-square methods. Main coefficients of the thermal expansion tensor were determined using *ThetaToTensor* program (Firsova et al. 2011).

Fig. 2 Back-scattered electron image of the sample containing $Na_2(Cu,Zn)Zn_2(SO_4)_4$ (NaCuZn, gray), $(Zn,Cu)_3O(SO_4)_2$ (ZnCu, white), $CuZn(SO_4)_2$ (CuZn, light-gray) and $Na_2Zn(SO_4)_2$ (NaZn, dark-gray)

HTXRD data (Fig. 3a) are consistent with thermal analysis data reported above. In general, the pattern does not undergo significant changes. $Na_2CuMg_2(SO_4)_4$ starts to decompose at 620 °C and peaks of CuO start to appear. Using data up to the decomposition we found a volumic dilatation coefficient $\alpha = 53 \cdot 10^{-6}$ °C which is rather high, in accordance with the rather "soft" framework offered by sulfates. However, this dilation is strongly anisotropic, as verified plotting the temperature dependence of the cell parameters (Fig. 3b) of $Na_2CuMg_2(SO_4)_4$ in the appropriate thermal range. They can be expressed by the following functions after fitting, where the temperature T is expressed in ℃:

$$a_t = 9.55759(59) + 0.1235(14) \times 10^{-3} T$$

$$b_t = 8.7675(10) + 0.0717(23) \times 10^{-3} T$$

$$c_t = 28.7345(86) + 0.330(58) \times 10^{-3} T + 0.885(84) \times 10^{-6} T^2$$

$$V_t = 2407.39(49) + 82(3) \times 10^{-3} T + 70(5) \times 10^{-6} T^2$$

Journal : Large 269 | Article No : 1132 | Pages : 14 | MS Code : 1132 | Dispatch : 28-12-2020

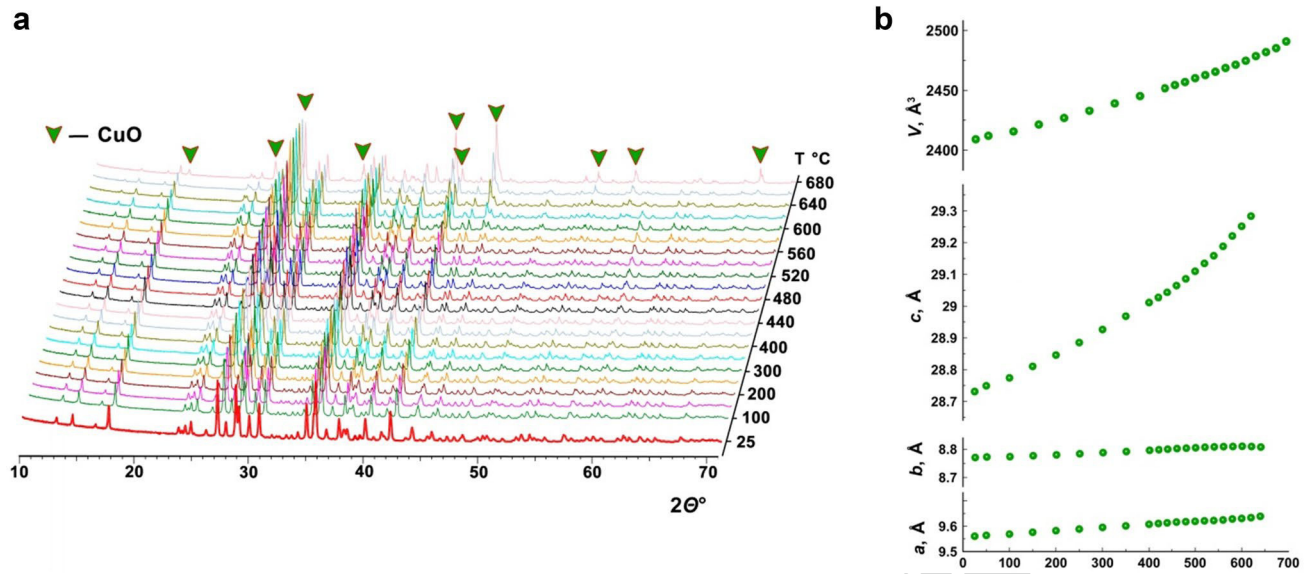

Fig. 3 Three-dimensional perspective plot showing all diffractograms for $Na_2CuMg_2(SO_4)_4$ over 10-75° 2Θ with increasing temperature (**a**). The temperature dependences of the unit-cell parameters and volume for $Na_2CuMg_2(SO_4)_4$ (**b**)

It is noteworthy that the most expanding direction is the *c*-axis giving the first experimental clue about a rather anisotropic and complex structural framework, as detailed below.

Single-crystal X-ray diffraction analysis

Single crystals of $Na_2CuMg_2(SO_4)_4$, $Na_2CuZn_2(SO_4)_4$ and $(Zn,Cu)_3O(SO_4)_2$ were mounted on thin glass fibers for X-ray diffraction analysis using Bruker APEX II DUO X-ray diffractometer with a microfocus X-ray tube operated with MoKα radiation at 50 kV and 0.6 mA. The data were integrated and corrected for absorption using a multiscan type model implemented in the Bruker program APEX2 (Bruker-AXS 2014). More than a hemisphere of X-ray diffraction data were collected for each crystal. Initial atomic coordinates for the crystal structures of $Na_2CuMg_2(SO_4)_4$ and $Na_2CuZn_2(SO_4)_4$ were taken from the structure of itelmenite (Nazarchuk et al. 2018). Both of the crystal structures were further refined in the *Pbca* space group to $R_1 = 0.036$ and $R_1 = 0.053$ for $Na_2CuMg_2(SO_4)_4$ and $Na_2CuZn_2(SO_4)_4$, respectively using the SHELXL program (Sheldrick 2015). Atomic coordinates reported for glikinite (Nazarchuk et al. 2020) were refined to $R_1 = 0.053$ in the crystal structure of $(Zn,Cu)_3O(SO_4)_2$. The main crystallographic information for all three new synthetic phases is summarized in Table 2. Selected interatomic distances are given in Tables 3 and 5.

Structure description

$Na_2CuMg_2(SO_4)_4$ and $Na_2CuZn_2(SO_4)_4$

There are three *M* sites (Fig. 4a), all coordinated by distorted octahedral arrays of O atoms with average *M*–O distances in the range, 2.08–2.17 Å (Table 3) in $Na_2CuMg_2(SO_4)_4$, $Na_2CuZn_2(SO_4)_4$ and itelmenite $Na_2CuMg_2(SO_4)_4$ (Nazarchuk et al., 2018). $M1O_6$ polyhedron has five *M*1–O bonds in the range 1.95–2.16 Å and sixth significantly longer *M*1-O bond ~ 2.8 Å. The similar coordination environments are also observed for *M*2 site. Thus, both *M*1 and *M*2 can be described as Jahn–Teller-distorted MO_{5+1} coordinations. *M*3 site has symmetrical [6O] octahedral coordination with two slightly elongated apical bonds of 2.15–2.29 Å. In general, substitution of Mg^{2+} ($r = 0.72$ Å) by Zn^{2+} ($r = 0.74$ Å) slightly increases *M*–O bond lengths. MO_6 polyhedra are characterized by the different degree of distortion (Table 4). The following Δ_{oct} bond-length distortion parameter, suggested in Wildner 1992, was used for octahedrally coordinated *M* sites in both $Na_2CuMg_2(SO_4)_4$ and $Na_2CuZn_2(SO_4)_4$: $\Delta_{oct} = \frac{1}{6}\sum_{i=1}^{6}\left[\frac{(d_i - d_m)}{d_m}\right]^2$ where $d_i = (M\text{–O})$ bond-length, $d_m = <M\text{–O}>$ bond-length (M = Cu, Mg, Zn). All of the *M*–O bonds ≤ 3 Å were taken into consideration (Table 3). Dealing with Mg^{2+} alkali earth against Cu^{2+} transition metal, the Δ_{oct} values correlate rather well with the content

Journal : Large 269 | Article No : 1132 | Pages : 14 | MS Code : 1132 | Dispatch : 28-12-2020

Table 2 Crystallographic data for $Na_2CuMg_2(SO_4)_4$, $Na_2CuZn_2(SO_4)_4$ and $(Zn,Cu)_3O(SO_4)_2$

	$Na_2CuMg_2(SO_4)_4$	$Na_2CuZn_2(SO_4)_4$	$(Zn,Cu)_3O(SO_4)_2$
Crystal system	Orthorhombic	Orthorhombic	Monoclinic
Space group	*Pbca*	*Pbca*	$P2_1/m$
Unit-cell dimensions			
a (Å)	9.531 (7)	9.458 (5)	7.3156 (6)
b (Å)	8.745 (6)	8.811 (4)	6.6004 (5)
c (Å)	28.71 (2)	28.850 (15)	7.8941 (7)
β (°)			117.424 (5)
Unit-cell volume (Å^3)	2393 (3)	2404 (2)	338.34 (5)
Z	4	4	2
Calculated density (g•cm^{-3})	3.032	3.450	3.968
Absorption coefficient (mm^{-1})	2.966	6.581	11.194
Crystal size (mm)	0.15×0.15×0.10	0.18×0.18×0.10	0.10×0.10×0.10
Data collection			
Temperature (K)	296(2)	296(2)	296(2)
Radiation, wavelength (Å)	Mo*K*α, 0.71073	Mo*K*α, 0.71073	Mo*K*α, 0.71073
θ range (°)	1.418—26.757	1.412—27.997	2.907–27.466
h, *k*, *l* ranges	− 8 → 12 − 11 → 8 − 36 → 36	− 12 → 10 − 11 → 8 − 36 → 38	− 12 → 10 − 11 → 8 − 36 → 38
Total reflections collected	10,945	12,574	848
Unique reflections (R_{int})	2532 (0.06)	2894 (0.12)	844(0.02)
Unique reflections $F > 4\sigma(F)$	1857	1679	783
Structure refinement			
Refinement method	Full-matrix least-squares on F^2	Full-matrix least-squares on F^2	Full-matrix least-squares on F^2
Weighting coefficients *a*, *b*	0.034500	0.048500	0.000200, 11.927700
Data/restraints/parameters	2532/0/230	2894/0/230	844/12/80
R_1 [$F > 4\sigma(F)$], wR_2 [$F > 4\sigma(F)$]	0.036, 0.074	0.053, 0.107	0.053, 0.105
R_2 all, wR_2 all	0.059, 0.083	0.113, 0.133	0.059, 0.108
Gof on F^2	1.006	0.958	1.144
Largest diff. peak and hole (*e* Å^{-3})	0.538, − 0.487	1.104, − 0.941	1.747,− 1.698

of Cu^{2+} cation in *M* sites due to the Cu^{2+} Jahn–Teller distortion. Cu:Mg ratio in *M* sites was obtained during the refinement of the crystal structure of $Na_2CuMg_2(SO_4)_4$ (Table 4). Cu^{2+} cation dominates in *M*1 site, whereas only 22.5% of copper is present in *M*2. The *M*3 site is almost completely occupied by Mg^{2+} cations in $Na_2CuMg_2(SO_4)_4$ in agreement with very symmetrical coordination environment.

The question of Cu^{2+} and Zn^{2+} cation distribution is significantly more difficult in $Na_2CuZn_2(SO_4)_4$, due to the very poor Cu/Zn scattering contrast by XRD. It can be only qualitatively (Table 4) partially answered on the basis of the different octahedral distortions of the Cu and Zn sites. Despite similar ionic radii, intuitively the Cu^{2+} Jahn–Teller effect is responsible for strong octahedral distortion. However, the second order Jahn–Teller effect which occurs for Zn^{2+} with a completely filled $3d^{10}$ shell (Boucher et al. 1994) can also lead to strong polyhedral distortion, such that Cu^{2+} for Zn^{2+} substitution in similar sites is possible. The strongest distortion is observed for $M1O_{5+1}$ octahedron in the crystal structures of both the mineral and its two synthetic analogs reported herein. The $M3O_6$ octahedron is obviously the least distorted preserving its main octahedral shape. Its $\Delta_{oct} \times 10^3$ value is close to 1 for $M3O_6$ in itelmenite and synthetic $Na_2CuMg_2(SO_4)_4$. ImportantlyΔ_{oct} is preserved for $M1O_{5+1}$ and $M2O_{5+1}$ despite distance changes in the latter and significantly increased for $M3O_6$ in $Na_2CuZn_2(SO_4)_4$, where it is expected to be mostly occupied by Zn^{2+}. According to these coordination changes after replacing Zn^{2+} for Mg^{2+}, Cu^{2+} cations are expected dominant in *M*1 site in $Na_2CuZn_2(SO_4)_4$, and in minor amount in *M*2 and *M*3.

Journal : Large 269 | Article No : 1132 | Pages : 14 | MS Code : 1132 | Dispatch : 28-12-2020

Table 3 Selected interatomic distances (in Å) in itelmenite (Nazarchuk et al. 2018), $Na_2CuMg_2(SO_4)_4$ and $Na_2CuZn_2(SO_4)_4$

Itelmenite				$Na_2CuMg_2(SO_4)_4$				$Na_2CuZn_2(SO_4)_4$			
*M*1–O14	1.961 (3)	Na2–O4	2.385 (3)	*M*1–O13	1.950 (3)	Na2–O4	2.376 (4)	*M*1–O13	1.962 (5)	Na2–O4	2.380 (6)
*M*1–O13	1.961 (3)	Na2–O13	2.447 (4)	*M*1–O14	1.956 (3)	Na2–O13	2.448 (4)	*M*1–O14	1.994 (6)	Na2–O14	2.428 (7)
*M*1–O16	1.976 (3)	Na2–O3	2.456 (3)	*M*1–O16	1.976 (3)	Na2–O3	2.459 (4)	*M*1–O16	2.024 (6)	Na2–O13	2.444 (7)
*M*1–O2	2.032 (3)	Na2–O14	2.465 (3)	*M*1–O2	2.023 (3)	Na2–O14	2.462 (4)	*M*1–O2	2.011 (6)	Na2–O7	2.462 (6)
*M*1–O3	2.153 (3)	Na2–O1	2.520 (3)	*M*1–O3	2.164 (3)	Na2–O7	2.530 (4)	*M*1–O3	2.116 (6)	Na2–O3	2.492 (7)
*M*1–O2	2.826 (3)	Na2–O7	2.544 (3)	*M*1–O2	2.804 (3)	Na2–O1	2.533 (4)	*M*1–O2	2.850 (6)	Na2–O1	2.533 (7)
<*M*1–O>	2.152	Na2–O10	2.828 (4)	<*M*1–O>	2.146	Na2–O10	2.829 (4)	<*M*1–O>	2.160	Na2–O15	2.812 (7)
		Na2–O15	2.846 (3)			Na2–O15	2.830 (4)			Na2–O10	2.868 (7)
*M*2–O11	1.980 (3)	<Na2–O>	2.561	*M*2–O11	1.962 (3)	<Na2–O>	2.558	*M*2–O11	1.981 (6)	<Na2–O>	2.552
*M*2–O8	2.028 (3)			*M*2–O8	2.005 (3)			*M*2–O8	2.021 (6)		
*M*2–O9	2.048 (3)	S1–O15	1.445 (3)	*M*2–O9	2.026 (3)	S1–O15	1.444 (3)	*M*2–O9	2.026 (6)	S1–O15	1.443 (6)
*M*2–O6	2.050 (3)	S1–O8	1.457 (3)	*M*2–O6	2.038 (3)	S1–O8	1.455 (3)	*M*2–O6	2.034 (5)	S1–O8	1.454 (6)
*M*2–O5	2.168 (3)	S1–O12	1.475 (3)	*M*2–O5	2.136 (3)	S1–O12	1.465 (3)	*M*2–O5	2.161 (6)	S1–O12	1.465 (6)
*M*2–O12	2.791 (3)	S1–O13	1.501 (3)	*M*2–O12	2.790 (4)	S1–O13	1.500 (3)	*M*2–O12	2.800 (7)	S1–O13	1.509 (6)
<*M*2–O>	2.178	<S1–O>	1.470	<*M*2–O>	2.160	<S1–O>	1.466	<*M*2–O>	2.171	<S1–O>	1.468
*M*3–O15	2.000 (3)	S2–O11	1.453 (3)	*M*3–O15	1.990 (3)	S2–O11	1.456 (3)	*M*3–O15	2.010 (6)	S2–O11	1.452 (6)
*M*3–O7	2.041 (3)	S2–O10	1.465 (3)	*M*3–O1	2.036 (3)	S2–O10	1.463 (3)	*M*3–O1	2.030 (5)	S2–O10	1.465 (6)
*M*3–O10	2.043 (3)	S2–O2	1.484 (3)	*M*3–O10	2.038 (3)	S2–O3	1.474 (3)	*M*3–O10	2.037 (5)	S2–O2	1.475 (6)
*M*3–O1	2.046 (3)	S2–O3	1.484 (3)	*M*3–O7	2.041 (3)	S2–O2	1.482 (3)	*M*3–O7	2.048 (6)	S2–O3	1.481 (5)
*M*3–O4	2.116 (3)	<S2–O>	1.472	*M*3–O4	2.127 (3)	<S2–O>	1.469	*M*3–O4	2.151 (6)	<S2–O>	1.468
*M*3–O12	2.211 (3)			*M*3–O12	2.222 (4)			*M*3–O12	2.288 (6)		
<*M*3–O>	2.076	S3–O7	1.465 (3)	<*M*3–O>	2.076	S3–O4	1.454 (3)	<*M*3–O>	2.094	S3–O4	1.469 (5)
		S3–O4	1.469 (3)			S3–O7	1.460 (3)			S3–O7	1.469 (6)
Na1–O3	2.393 (3)	S3–O1	1.470 (2)	Na1–O3	2.375 (4)	S3–O1	1.467 (3)	Na1–O3	2.405 (6)	S3–O1	1.480 (5)
Na1–O16	2.480 (4)	S3–O14	1.487 (3)	Na1–O16	2.488 (4)	S3–O14	1.490 (3)	Na1–O16	2.480 (7)	S3–O14	1.486 (6)
Na1–O5	2.493 (3)	<S3–O>	1.473	Na1–O5	2.516 (4)	<S3–O>	1.468	Na1–O5	2.485 (7)	<S3–O>	1.476
Na1–O6	2.528 (3)			Na1–O6	2.525 (4)			Na1–O6	2.486 (7)		
Na1–O13	2.725 (4)	S4–O5	1.462 (3)	Na1–O13	2.683 (4)	S4–O5	1.451 (3)	Na1–O13	2.686 (7)	S4–O5	1.451 (5)
Na1–O2	2.756 (3)	S4–O9	1.468 (3)	Na1–O2	2.728 (4)	S4–O9	1.468 (3)	Na1–O2	2.739 (7)	S4–O9	1.466 (6)
Na1–O8	2.876 (4)	S4–O6	1.480 (3)	Na1–O8	2.857 (4)	S4–O16	1.475 (3)	Na1–O8	2.743(7)	S4–O16	1.483 (6)
Na1–O9	2.879 (4)	S4–O16	1.483 (3)	Na1–O9	2.883 (4)	S4–O6	1.481 (3)	Na1–O9	2.888(7)	S4–O6	1.486 (6)
Na1–O16	3.134 (4)	<S4–O>	1.473	Na1–O16	3.108 (4)	<S4–O>	1.469	Na1–O16	3.142 (7)	<S4–O>	1.472
Na1–O6	3.155 (4)			Na1–O6	3.175 (4)			Na1–O6	3.250 (7)		
<Na1–O>	2.742			<Na1–O>	2.734			<Na1–O>	2.730		

Journal : Large 269 | Article No : 1132 | Pages : 14 | MS Code : 1132 | Dispatch : 28-12-2020

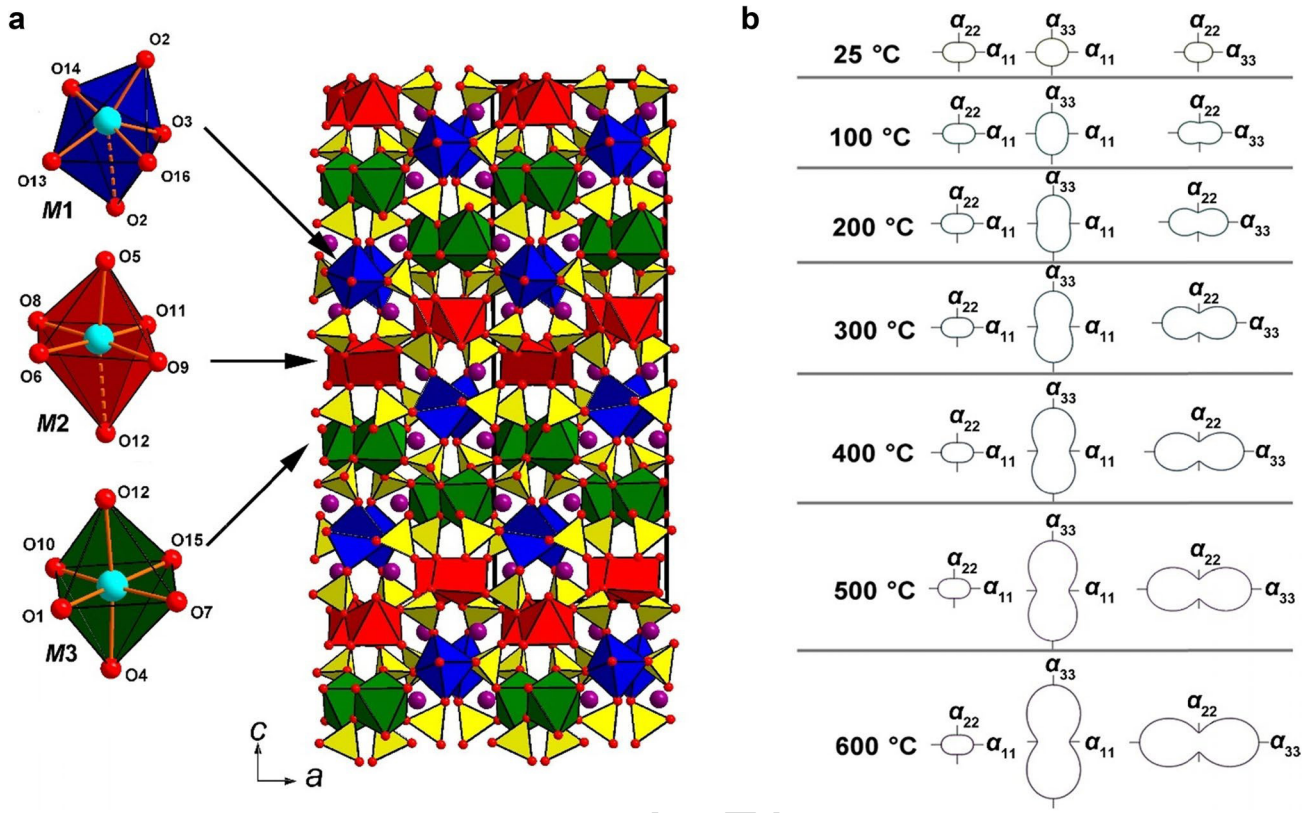

Fig. 4 Coordination of *M* sites in $CuMg_2O(SO_4)_2$ and $CuZn_2O(SO_4)_2$ (distances < 2.5 Å are shown by dashed lines) (left) and general projection of the crystal structure of $Na_2CuMg_2(SO_4)_4$ along the *b* axis (weak Cu–O bonds > 2.5 Å are omitted for clarity) (**a**). Pole figures of the thermal expansion coefficients of $Na_2CuMg_2(SO_4)_4$ at different temperatures (**b**)

Table 4 Selected interatomic distances (in Å) in glikinite (Nazarchuk et al. 2020) and $(Zn,Cu)_3O(SO_4)_2$

Glikinite				$(Zn,Cu)_3O(SO_4)_2$			
*M*1–O1	1.878 (5)×2	S1–O7	1.361 (15)	*M*1–O1	1.878 (4)×2	S1–O7	1.406 (18)
*M*1–O2	2.191 (10)×2	S1–O6	1.435 (18)	*M*1–O2	2.206 (9)×2	S1–O6	1.41 (2)
*M*1–O4	2.230 (10)×2	S1–O4	1.465 (13)×2	*M*1–O4	2.233 (10)×2	S1–O4	1.473 (10)×2
<*M*1–O>	2.100	<S1–O>	1.432	<M1–O>	2.105	<S1–O>	1.441
*M*2–O6	1.902 (17)	S2–O3	1.413 (14)	*M*2–O6	1.91 (2)	S2–O3	1.453 (11)
*M*2–O1	1.939 (12)	S2–O5	1.435 (13)	*M*2–O1	1.956 (12)	S2–O5	1.481 (12)
*M*2–O3	1.967 (14)	S2–O2	1.480 (12)×2	*M*2–O3	1.982 (13)	S2–O2	1.465 (10)×2
*M*2–O2	2.153 (13)×2	<S2–O>	1.451	*M*2–O2	2.165 (10)×2	<S2–O>	1.466
<M2–O>	2.023			<M2–O>	2.036		
		O1–*M*1	1.878 (5)×2			O1–*M*1	1.878 (4)×2
*M*3–O7	1.938 (15)	O1–*M*2	1.939 (12)	*M*3–O7	1.906 (19)	O1–*M*2	1.982 (13)
*M*3–O5	1.977 (14)	O1–*M*3	1.987 (13)	*M*3–O5	1.966 (13)	O1–*M*3	1.966 (13)
*M*3–O1	1.987 (13)	<O1–M>	1.921	*M*3–O1	1.966 (12)	<O1–*M*>	1.926
*M*3–O4	2.144 (15)×2			*M*3–O4	2.149 (11)×2		
<*M*3–O>	2.038			<*M*3–O>	2.027		

There are two positions fully occupied by Na in $Na_2CuMg_2(SO_4)_4$ and $Na_2CuZn_2(SO_4)_4$. Na1 atom forms ten Na–O bonds in the range 2.38–3.25 Å, whereas Na2 is coordinated by the eight O atoms in the range 2.38–2.87 Å. In the crystal structure of natural itelmenite (Nazarchuk et al. 2018), admixture of K is concentrated in Na1 site with the larger coordination sphere.

Journal : Large 269 | Article No : 1132 | Pages : 14 | MS Code : 1132 | Dispatch : 28-12-2020

Table 5 *M* site populations and $\Delta_{oct} \times 10^{-3}$ in the structures of itelmenite, $Na_2CuMg_2(SO_4)_4$ and $Na_2CuZn_2(SO_4)_4$

	Itelmenite (Nazarchuk et al. 2018)	$\Delta_{oct} \times 10^{-3}$	$Na_2CuMg_2(SO_4)_4$	$\Delta_{oct} \times 10^{-3}$	$Na_2CuZn_2(SO_4)_4$	$\Delta_{oct} \times 10^{-3}$
*M*1	$Cu_{0.71}Mg_{0.09}Zn_{0.2}$	20.62	$Cu_{0.820(5)}Mg_{0.180(5)}$	19.98	Cu > Zn	20.92
*M*2	$Mg_{0.55}Cu_{0.39}Zn_{0.06}$	16.55	$Mg_{0.775(4)}Cu_{0.225(4)}$	17.64	Zn > Cu	17.48
*M*3	$Mg_{0.91}Zn_{0.09}$	1.11	$Mg_{0.949(3)}Cu_{0.051(3)}$	1.38	Zn > Cu	2.18

Four symmetrically independent S^{6+} cations show very similar S–O bond lengths in itelmenite and $Na_2CuMg_2(SO_4)_4$, $Na_2CuZn_2(SO_4)_4$. The < S–O > distances demonstrate very similar values of ~1.47 Å.

The structural architecture of $Na_2CuMg_2(SO_4)_4$ and $Na_2CuZn_2(SO_4)_4$ is simple, where each of the vertices of the SO_4 tetrahedron is common with one of the vertices of the MO_6 octahedron. Resulted system of channels in the framework is filled by Na^+ cations (Fig. 4b). Itelmenite-type structural topology is unknown in synthetic compounds.

High-temperature powder X-ray diffraction studies (Fig. 3) show that $[CuMg_2(SO_4)_4]^{2-}$ framework upon heating expands anisotropically (Fig. 4b). Note that, at room temperature expansion is almost isotropic. The thermal expansion occurs mostly in the direction of α_{33}.

$(Zn,Cu)_3O(SO_4)_2$

There are three *M* sites (Table 5) in the structure of synthetic analog of glikinite. Refinement of the crystal structure is complicated by the presence of the significant amount of Cu^{2+} (see chemical composition above) distributed over *M* sites. *M*1 site has slightly distorted octahedral coordination with $\Delta_{oct} \times 10^{-3} = 5.87$. Relatively small value indicates only minor presence of Cu^{2+} in $M1O_6$ octahedron. *M*2 and *M*3 sites are 5-coordinated (Fig. 5a). Addison tau-parameter has been used to describe the distortion around *M*2 and *M*3 sites. Values of $\tau = 0.41$ and $\tau = 0.35$ for *M*2 and *M*3 sites, respectively, were calculated. Thus coordination environments of both sites are intermediate from square pyramidal to trigonal bipyramidal geometry. $M2O_5$ and $M3O_5$ coordinations are more typical for Cu^{2+} rather than to Zn^{2+}. The question of the distribution of Cu^{2+} and Zn^{2+} in glikinite and its synthetic analog remains a debate.

Average S–O bond lengths show typical values of 1.441 and 1.466 Å for the $S1O_4$ and $S2O_4$ tetrahedra, respectively.

The structure of $(Zn,Cu)_3O(SO_4)_2$ contains seven O^{2-} anions. The O2-O7 are strongly bonded in SO_4^{2-} groups. The O1 atom is tetrahedrally coordinated by four Zn^{2+}, Cu^{2+} cations, forming short and strong O-Zn bonds. From the viewpoint of bond valence theory, these bonds are the strongest in the structure and thus it makes absolute sense to consider the O1 atoms as centers of oxocentered $O(Zn,Cu)_4$ tetrahedra. The mean O-Zn length in the $O1Zn_4$ tetrahedron

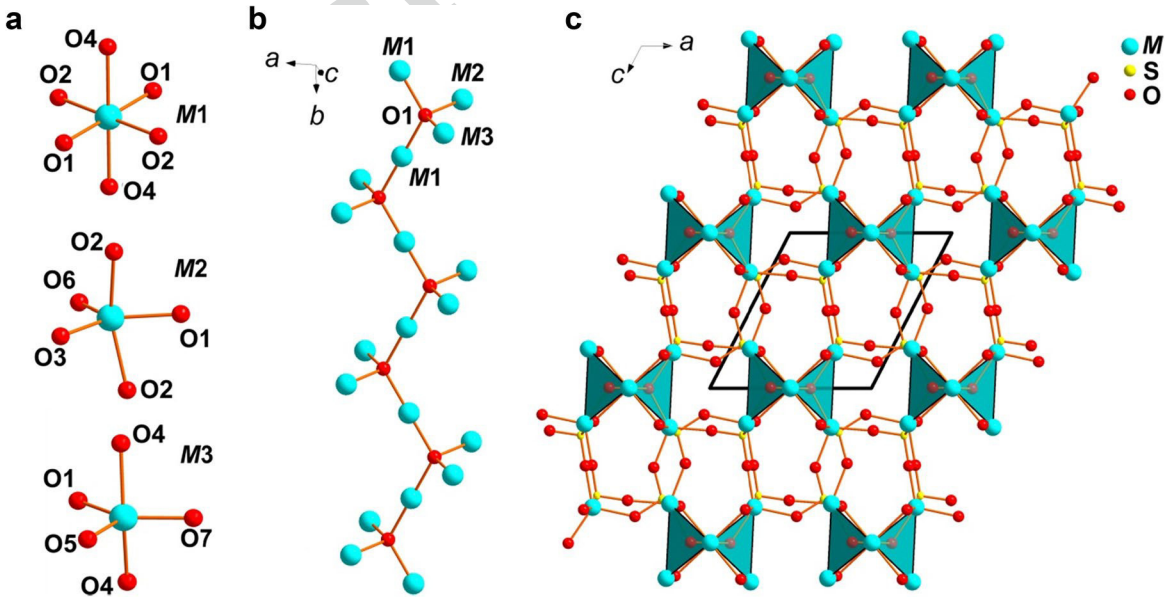

Fig. 5 Coordination of *M* sites in $(Zn,Cu)_3O(SO_4)_2$ (**a**). $[M_3O]^{2+}$ chain elongated along the *b* axis (**b**). General projection of the crystal structure of $(Zn,Cu)_3O(SO_4)_2$ (**c**). $[M_3O]^{2+}$ chains are highlighted by blue

is 1.926 Å, which is typical for such units (Krivovichev et al. 2013) taking into account high content of Cu^{2+}. The $O(Zn,Cu)_4$ tetrahedra link together via common vertices to form $[(Zn,Cu)_3O]^{4+}$ single chains (Fig. 5b). In this unit, each tetrahedron shares two of four vertices with adjacent tetrahedra. The $[(Zn,Cu)_3O]^{4+}$ single chains extend along the *b* axis. Oxocentered chains are interconnected via SO_4 groups into framework projected in Fig. 5c.

Evaluation of Na^+-ion diffusion in $Na_2CuM_2(SO_4)_4$ (M = Mg, Zn)

The BVEL iso-energy surfaces were generated based on the structural data of the synthetic $Na_2CuMg_2(SO_4)_3$ phase using the BondStr program (FullProf Suite (Rodríguez-Carvajal, 1993)). Figure 6 demonstrates calculated possible Na^+ diffusion pathways in $Na_2CuM_2(SO_4)_4$ considering all counterions at distances up to 8 Å and the polarizability of Na^+. An energy of 1.6 eV is usually considered as required percolation energy for the diffusion of Na^+ in conducting polyanionic compounds (Sun et al. 2015; Boivin et al. 2016; Kovrugin et al. 2018). In the framework of $Na_2CuM_2(SO_4)_4$, the iso-energy surface of 1.6 eV represents a non-interconnected ion diffusion path (Fig. 6a) indicating a limited Na^+ diffusion inside the structure. The energy level leading to an infinitely connected surface for Na^+ diffusion in $Na_2CuM_2(SO_4)_4$ corresponds only to 3.0 eV above the minimum energy level (Fig. 6b), which is a rather high energy barrier far above the expected BVEL calculations of $E_m < 1.5$ eV for any fast ion conductor (Katcho et al 2019) and, thus, the $Na_2CuM_2(SO_4)_4$ framework cannot be considered as a good Na^+ conductor. Meanwhile, it should be noted that a lithiated analog of the structure can probably induce a higher ionic conductivity (Boivin et al. 2017).

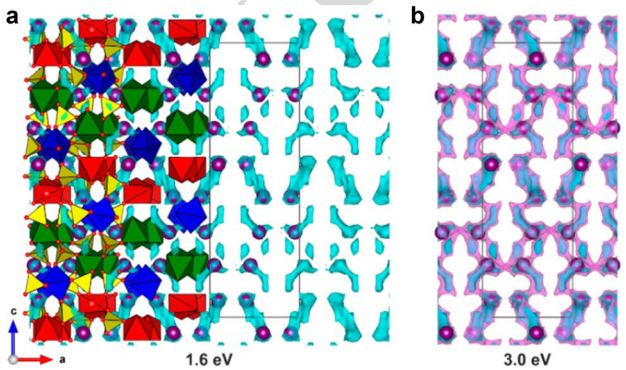

Fig. 6 Na^+-ion diffusion pathways obtained using bond valence energy landscapes with an iso-energy surface value of 1.6 eV (**a**) and 3.0 eV (**b**) above the minimum energy level. The iso-energy surfaces of 1.6 and 3.0 eV are shown by cyan and pink, respectively. Legend for the unit-cell content see in Fig. 4

Low conductive ability of the $Na_2CuM_2(SO_4)_4$ framework is not surprising, since there is a number of works reporting a limited ion diffusion inside sulfate polyanionic structures (Lander et al. 2017; Kovrugin et al. 2019). However, we believe that the sulfate-based cathodes have a commercial potential in future considering a higher electronegative nature of sulfur, which may deliver the highest redox potential and lead to formation of cathode materials offering high voltage operation and, thus, competitive energy density overcoming weight penalties and lower theoretical capacity in comparison with conventional oxide cathodes.

Discussion

Our experiments indicate that investigation of anhydrous sulfate systems reproduces many compounds known before as mineral species only. It appeared possible to obtain the Zn- and Mg-analogs of itelmenite. Moreover, the latter was obtained as a pure phase which allowed the study of thermal expansion. The possibility of the formation of synthetic analogs of puninite $Na_2Cu_3O(SO_4)_2$ (Siidra et al. 2017), hermannjahnite $CuZn(SO_4)_2$ (Siidra et al. 2018) and glikinite $Zn_3O(SO_4)_2$ (Nazarchuk et al. 2020) as side products has been shown. On the other hand, the presence of $Na_2Zn(SO_4)_2$ compound (Berg and Thorup 2005) among the crystallized phases, unknown to date as a mineral, shows a high probability of finding such a mineral species in the fumaroles of the scoria cones of the Tolbachik volcano. Note that all the compounds synthesized in our work were obtained by the method of solid-state reactions in open air, and not from gas as in natural mineral forming fumarolic environments. AQ9

Earlier, in Nazarchuk et al. (2018), we have suggested that itelmenite may form as a result of the interaction between gas and basalt scoria. This hypothesis is confirmed by the syntheses and phase formation described above. Mg and possibly Na components in the fumarole come from the scoria, not from the gases. The concentrations of metals in the Tolbachik gases, during recent 2012–2013 eruption, are higher than the corresponding concentrations in high-temperature fumaroles worldwide (Zelenski et al. 2014). The hot Cu, Zn and sulfate bearing fumarolic gases condense on AQ10 the surfaces of the scoria, forming a liquid which dissolves Na and Mg species from the basaltic scoria which then crystallize once the temperature is sufficiently low. Our study shows that outstanding mineralogical diversity observed in the fumaroles of scoria cones is not only due to the formation from the gas enriched by transition metals and involves also intensive exchange with the host basaltic scoria. The similar processes seem also to be responsible for the recrystallization of silicates described from deep and hot zones of Arsenatnaya fumarole (Shchipalkina et al. 2020).

Journal : Large 269 | Article No : 1132 | Pages : 14 | MS Code : 1132 | Dispatch : 28-12-2020

The phase formation in the system with Mg turned out to be interesting and very different from the system with Zn. Apparently, such a difference can be explained by much lower melting point of $ZnSO_4$ (680 °C) compared with $MgSO_4$ (1137 °C). In addition, zinc has crystal chemical affinity with divalent copper, which leads to a greater structural diversity of the newly formed phases and more complex phase diagrams not available to date.

$Zn_3O(SO_4)_2$ phase was previously described by Bald and Grühn (1981). Interestingly, the polyhedra of zinc in the previously described Cu-free synthetic compound and the polyhedra with a significant admixture of copper in the $(Zn,Cu)_3O(SO_4)_2$ described above and glikinite demonstrate very similar bond lengths and overall geometry. Jahn–Teller effect of Cu^{2+} in octahedral environment and the second order Jahn–Teller effect of Zn^{2+} result in distortions of similar magnitude (Halcrow 2013).

In our opinion, a significant amount of copper is important for the stabilization of this structure type and the formation of oxocentered $[(Zn,Cu)_3O]^{4+}$ units. Admixture of Cu^{2+} also controls the formation of itelmenite-type phases.

Acknowledgements We are grateful to Tonči Balić-Žunić, Wulf Depmeier and an anonymous reviewer for valuable comments. This work was financially supported by the Russian Science Foundation through the grant 16-17-10085. Technical support by the SPbSU X-ray Diffraction and Geomodel Resource Centers is gratefully acknowledged. The Chevreul Institute (FR 2638), the Ministère de l'Enseignement Supérieur et de la Recherche, the Région Hauts-de-France, the CNRS, and the FEDER are acknowledged for supporting and funding this work.

References

Alpers C, Jambor J, Nordstrom D. (Eds.) (2000) Sulfate Minerals. Crystallography, Geochemistry, and Environmental Significance. Rev Mineral Geochem 40:608 p

Bald L, Grühn R (1981) Die Kristallstruktur von einem Sulfat-reichen Oxidsulfat des Zinks. Naturwissenschaften 68:39–39

Balić Žunić T, Garavelli A, Acquafredda P, Leonardsen E, Jakobsson SP (2009) Eldfellite, a new fumarolic mineral from Eldfell volcano, Iceland. Mineral Mag 73:51–57

Barpanda P (2015) Sulfate chemistry for high-voltage insertion materials: synthetic, structural and electrochemical insights. Isr J Chem 55:537–557

Barpanda P, Oyama G, Nishimura S, Chung S-C, Yamada A (2014) A 3.8-V earth-abundant sodium battery electrode. Nat Commun 5:4358

Belousov A, Belousova M, Edwards B, Volynets A, Melnikov D (2015) Overview of the precursors and dynamics of the 2012–13 basaltic fissure eruption of Tolbachik Volcano, Kamchatka, Russia. J Volcanol Geoth Res 307:22–37

Berg RW, Thorup N (2005) The reaction between ZnO and molten $Na_2S_2O_7$ or $K_2S_2O_7$ forming $Na_2Zn(SO_4)_2$ or $K_2Zn(SO_4)_2$, studied by Raman spectroscopy and X-ray diffraction. Inorg Chem 44:3485–3493

Boivin E, Chotard J-N, Ménétrier M, Bourgeois L, Bamine T, Carlier D, Fauth F, Suard E, Masquelier C, Croguennec L (2016) Structural and electrochemical studies of a new Tavorite composition: $LiVPO_4OH$. J Mater Chem A4:11030–11045

Boivin E, Chotard J-N, Bamine T, Carlier D, Serras P, Palomares V, Rojo T, Iadecola A, Dupont L, Bourgeois L, Fauth F, Masquelier C, Croguennec L (2017) Vanadyl-type defects in Tavorite-like $NaVPO_4F$: from the average long range structure to local environments. J Mater Chem A5:25044–25055

Boucher F, Evain M, Brec R (1994) Second-order Jahn-Teller effect in $CdPS_3$ and $ZnPS_3$ demonstrated by a non-harmonic behaviour of Cd^{2+} and Zn^{2+} d^{10} ions. J Alloy Compd 215:63–70

Bruker-AXS (2014) APEX2. Version 2014.11–0. Madison, Wisconsin, USA

Chaplygin I, Lavrushin V, Dubinina E, Bychkova YV, Inguaggiato S, Yudovskaya M (2016) Geochemistry of volcanic gas at the 2012–13 New Tolbachik eruption, Kamchatka. J Volcanol Geoth Res 323:186–193

Fedotov SA, Markhinin YK (eds) (1983) The Great Tolbachik Fissure Eruption. Cambridge Univ. Press, New York

Firsova VA, Bubnova RS, Filatov SK (2011) Program for the thermal expansion tensor determination for crystalline materials. Institute of Silicate Chemistry of Russ. Acad. Sci, St. Petersburg, Russia

Halcrow MA (2013) Jahn-Teller distortions in transition metal compounds, and their importance in functional molecular and inorganic materials. Chem Soc Rev 42:1784–1795

Katcho NA, Carrete J, Reynaud M, Rousse G, Casas-Cabanas M, Mingo N, Rodríguez-Carvajal J, Carrasco J (2019) An investigation of the structural properties of Li and Na fast ion conductors using high-throughput bond-valence calculations and machine learning. J Appl Cryst 52:148–157

Kovrugin VM, David R, Chotard J-N, Recham N, Masquelier C (2018) A high voltage cathode material for sodium batteries: $Na_3V(PO_4)_2$. Inorg Chem 57:8760–8768

Kovrugin VM, Nekrasova DO, Siidra OI, Mentré O, Masquelier C, Stefanovich SY, Colmont M (2019) Mineral-inspired crystal growth and physical properties of $Na_2Cu(SO_4)_2$ and review of $Na_2M(SO_4)_2(H_2O)_x$ (x = 0–6) compounds. Cryst Growth Des 19:1233–1244

Krivovichev SV, Mentré O, Siidra OI, Colmont M, Filatov SK (2013) Anion-centered tetrahedra in inorganic compounds. Chem Rev 113:6459–6535

Lander L, Rousse G, Batuk D, Colin CV, Dalla Corte DA, Tarascon J-M (2017) Synthesis, structure, and electrochemical properties of K-based sulfates $K_2M_2(SO_4)_3$ with M = Fe and Cu. Inorg Chem 56:2013–2021

Lander L, Tarascon J-M, Yamada A (2018) Sulfate-based cathode materials for Li- and Na-ion batteries. Chem Rec 18:1394–1408

Nazarchuk EV, Siidra OI, Agakhanov AA, Lukina EA, Avdontseva EY, Karpov GA (2018) Itelmenite, $Na_2CuMg_2(SO_4)_4$, a new anhydrous sulphate mineral from the Tolbachik volcano. Mineral Mag 82:1233–1241

Nazarchuk EV, Siidra OI, Nekrasova DO, Shilovskikh VV, Borisov AS, Avdontseva EYu (2020) Glikinite, $Zn_3O(SO_4)_2$, a new anhydrous zinc oxysulphate mineral structurally based on OZn_4 tetrahedra. Mineral Mag 84:563–567

Pautov LA, Mirakov MA, Siidra OI, Faiziev AR, Nazarchuk EV, Karpenko VYu, Makhmadsharif S (2020) Falgarite, $K_4(VO)_3(SO_4)_5$, a new mineral from sublimates of a natural underground coal fire at the tract of Kukhi-Malik, Fan-Yagnob coal deposit, Tajikistan. Mineral Mag 84:455–462

Pekov IV, Koshlyakova NN, Zubkova NV, Lykova IS, Britvin SN, Yapaskurt VO, Agakhanov AA, Shchipalkina NV, Turchkova AG, Sidorov EG (2018a) Fumarolic arsenates - a special type of arsenic mineralization. Eur J Mineral 30:305–322

Pekov IV, Zubkova NV, Pushcharovsky DYu (2018b) Copper minerals from volcanic exhalations—a unique family of natural compounds: crystal-chemical review. Acta Crystallogr B 74:502–518

Petříček V, Dušek M, Palatinus L (2014) Crystallographic computing system JANA2006: general features. Z Kristallogr Cryst Mater 229:345–352

Rodríguez-Carvajal J (1993) Recent advances in magnetic structure determination by neutron powder diffraction. Phys B 192:55–69

Secco EA (1988) Spectroscopic properties of SO_4 (and OH) in different molecular and crystalline environments. I. Infrared spectra of $Cu_4(OH)_6SO_4$, $Cu_4(OH)_4OSO_4$, and $Cu_3(OH)_4SO_4$. Can J Chem 66:329–336

Sharygin VV, Sokol EV, Belakovski DI (2009) Fayalite-sekaninaite paralava from the Ravat coal fire (central Tajikistan). Russ Geol Geophys 50:703–721

Shchipalkina NV, Pekov IV, Koshlyakova NN, Britvin SN, Zubkova NV, Varlamov DA, Sidorov EG (2020) Unusual silicate mineralization in fumarolic sublimates of the Tolbachik volcano, Kamchatka, Russia—Part 1: Neso-, cyclo-, ino- and phyllosilicates. Eur J Mineral 32:101–119

Sheldrick GM (2015) Crystal structure refinement with SHELXL. Acta Crystalogr C71:3–8

Siidra OI, Nazarchuk EV, Zaitsev AN, Lukina EA, Avdontseva EY, Vergasova LP, Vlasenko NS, Filatov SK, Turner R, Karpov GA (2017) Copper oxosulphates from fumaroles of Tolbachik Vulcano: puninite, $Na_2Cu_3O(SO_4)_3$—a new mineral species and structure refinements of kamchatkite and alumoklyuchevskite. Eur J Mineral 29:499–510

Siidra OI, Nazarchuk EV, Agakhanov AA, Lukina EA, Zaitsev AN, Turner R, Filatov SK, Pekov IV, Karpov GA, Yapaskurt VO (2018) Hermannjahnite, $CuZn(SO_4)_2$, a new mineral with chalcocyanite derivative structure from the Naboko scoria cone of the 2012–2013 fissure eruption at Tolbachik volcano, Kamchatka, Russia. Miner Petrol 112:123–134

Siidra OI, Borisov AS, Lukina EA, Depmeier W, Platonova NV, Colmont M, Nekrasova DO (2019) Reversible hydration/dehydration and thermal expansion of euchlorine, ideally $KNaCu_3O(SO_4)_3$. Phys Chem Miner 46:403–416

Singh P, Shiva K, Celio H, Goodenough JB (2015) Eldfellite, $NaFe(SO_4)_2$: an intercalation cathode host for low-cost Na-ion batteries. Energ Environ Sci 8:3000–3005

Smith DH, Seshadri KS (1999) Infrared spectra of $Mg_2Ca(SO_4)_3$, $MgSO_4$, hexagonal $CaSO_4$, and orthorhombic $CaSO_4$. Spectrochim Acta A55:795–805

Sun M, Rousse G, Abakumov AM, Saubanère M, Doublet M-L, Rodríguez-Carvajal J, Van Tendeloo G, Tarascon J-M (2015) $Li_2Cu_2O(SO_4)_2$: a possible electrode for sustainable Li-based batteries showing a 4.7 V redox activity vs Li^+/Li^0. Chem Mater 27:3077–3087

Vergasova LP, Filatov SK (2012) New mineral species in products of fumarole activity of the Great Tolbachik Fissure Eruption. J Volcanol Seismol 6:281–289

Wildner M (1992) On the geometry of $Co(II)O_6$ polyhedra in inorganic compounds. Z Kristallogr 202:51–70

Zelenski M, MalikTaran NY (2014) Emissions of trace elements during the 2012–2013 effusive eruption of Tolbachik volcano, Kamchatka: enrichment factors, partition coefficients and aerosol contribution. J Volcanol Geotherm Res 285:136–149

Journal:	**269**
Article:	**1132**

Author Query Form

Please ensure you fill out your response to the queries raised below and return this form along with your corrections

Dear Author

During the process of typesetting your article, the following queries have arisen. Please check your typeset proof carefully against the queries listed below and mark the necessary changes either directly on the proof/online grid or in the 'Author's response' area provided below

Author Proof

Query	Details Required	Author's Response
AQ1	Author: Please check and confirm that the authors and their respective affiliations have been correctly identified and amend if necessary.	
AQ2	Please check and confirm the edit made in Article title.	
AQ3	Author: Kindly provide complete details for reference Alpers et al. 2000.	
AQ4	Is the usage 'Naboko' correct? Please check and amend if necessary.	
AQ5	Author: Part label c is missing in figure caption 1. Please check.	
AQ6	Two different representation of 'Zn-Cu' and 'ZnCu' are found throughout the article. Please check and amend if necessary.	
AQ7	Author: Figure [2] was received; however, no citation was provided in the manuscript. Please check and confirm the inserted citation of Fig/Table is correct. If not, please suggest an alternative citation. Please note that figures and tables should be cited in ascending numerical order in the text. and should be inside the main body of the text.	
AQ8	Is the usage 'volumic' correct? Please check and amend if necessary.	
AQ9	Author: Please check the layout of Table 1, and correct if necessary.	
AQ10	AUTHOR: Zelensky et al. 2014 has been changed to Zelenski et al., 2014 so that this citation matches the Reference List. Please confirm that this is correct.	